



Liu, Y., Li, Z., Xiao, Z., Yin, H., Li, X. and He, T. (2020) Synergy of slippery surface and pulse flow: An anti-scaling solution for direct contact membrane distillation. *Journal of Membrane Science*, 603, 118035. (doi: [10.1016/j.memsci.2020.118035](https://doi.org/10.1016/j.memsci.2020.118035)).

This is the author's final accepted version.

There may be differences between this version and the published version. You are advised to consult the publisher's version if you wish to cite from it.

<http://eprints.gla.ac.uk/226461/>

Deposited on: 24 November 2020

Enlighten – Research publications by members of the University of Glasgow
<http://eprints.gla.ac.uk>

1
2
3
4
5
6
7
8
9
10
11
12
13
14
15
16
17
18
19

**Synergy of slippery surface and pulse flow: an anti-scaling solution
for direct contact membrane distillation**

Yongjie Liu ^{a,b,c}, Zhansheng Li ^d, Zechun Xiao ^{a,c}, Huabing Yin ^e, Xuemei Li^a, Tao He^{a*}

^aShanghai Advanced Research Institute, Chinese Academy of Sciences, Shanghai 201210, China

^bSchool of Physical Science and Technology, ShanghaiTech University, Shanghai 201210, China

^cUniversity of Chinese Academy of Sciences, Beijing 100049, China

^dNational Key Laboratory of Fine Chemical Engineering, Department of Polymer Materials,
Dalian University of Technology, Dalian 116024, China

^eSchool of Engineering, University of Glasgow, Glasgow, G12 8LT, UK

*Corresponding authors: het@sari.ac.cn

Abstract

Recent progress on mitigating scaling on hydrophobic membrane distillation (MD) membrane focuses on the design of superhydrophobic/omniphobic surface and process optimization. However, the rationale for scaling resistance is not yet complete. We attempted in this work to unravel the correlation of scaling resistance based on the synergy of slippery surface (via chemical engineering) and pulse flow (process engineering). Superhydrophobic micro-pillared polyvinylidene fluoride (MP-PVDF) and CF_4 plasma modified MP-PVDF (CF_4 -MP-PVDF) were utilized as the model membranes. We proposed rheometry as a simple quantitative measure for the wetting state in a hydrodynamic environment. Results showed that MP-PVDF possessed pinned wetting and prone to scaling (2000 mg/L CaSO_4 solution) in both steady and pulse flow. In contrast, the CF_4 -MP-PVDF showed suspended wetting and excellent scaling resistance (at water recovery of 60 %, the CF_4 -MP-PVDF surface was still clean without any crystals) under pulse flow, but not at steady flow. At steady flow, feed over-pressure changes the suspended wetting to pinned wetting by pushing the water-gas interface into the pillars, thereby resulting in scaling for CF_4 -MP-PVDF. At pulse flow, rhythmic fluctuation in the water-gas interface for CF_4 -MP-PVDF led to sustained scaling resistance. For the first time, we experimentally demonstrated a scaling resistance in DCMD via engineering surface wetting state and process. We envision that this rationale would pave the forward-looking strategy for a robust stable MD process in the near future.

Keywords: Superhydrophobic; Slippery; Scaling; Suspended wetting; Pinned wetting

40

41 **1. Introduction**

42 Membrane distillation (MD) is a thermal desalination process which utilizes microporous
43 hydrophobic membrane [1, 2]. As a desalination process that can utilize low-grade heat to treat
44 highly saline brine, MD has been actively explored as a promising technology for saltwater
45 management and zero liquid discharge (ZLD) [3, 4]. Managing hypersaline brine is a key
46 environmental challenge because reverse osmosis (RO) is not applicable when the brine osmotic
47 pressure exceeds the current allowable working pressure of the RO system [5, 6]. In contrast, the
48 performance of MD is basically independent of the brine salinity, theoretically allowing MD to
49 achieve a high brine volume reduction up to saturation and crystallization [7]. The inevitable
50 challenge of this application is scaling, as the formation or deposition of mineral crystals on the
51 membrane surface, which ultimately leads to a complete process failure [8, 9].

52 Scaling poses a detrimental effect on MD performance by blockage of membrane pores and
53 reduction in permeance due to homogeneous and heterogeneous nucleation of inorganics [10].
54 Homogeneous nucleation is difficult which requires supersaturation and sometimes seeding.
55 Comparably, heterogeneous nucleation is relatively easy to occur at the membrane surface. The
56 strategy to largely constrain the formation of crystal scaling on the membrane surface is to increase
57 the membrane hydrophobicity, thus reduce the surface energy or increase the heterogeneous
58 nucleation energy [11].

59 Classical nucleation theory assumes that low surface energy is the most important governing
60 factor for mitigating scaling [12-15]. Recently, superhydrophobic surface and omniphobic surfaces

61 were researched as an important means for scaling and fouling mitigation [16-20]. Besides efforts
62 on the membrane surface characteristics, there were also researches focused on process controls,
63 such as ultrasonic enhancement [21], gas bubbling [22] and microbubble aeration [23]. Results
64 from Lin's group show that a synergistic combination of superhydrophobic membrane and gas
65 purging leads to effective mitigation of membrane scaling [24]. Process Engineering of periodic
66 air backwashing from the distillate side to the feed side has proved to be effective and practically
67 feasible to reduce the membrane scaling [24-26]. However, the process has to be paused and
68 modules have to be drained. An extra blower is required which complicates the system. In this
69 work, we will investigate a facile approach to achieve sustained, stable MD operation with
70 excellent scaling resistance.

71 The rationale of our aim is based on the findings of a hydrodynamic factor of slippage at the
72 superhydrophobic membrane/air/liquid interface. The finding was based on precisely designed
73 micro-pillared PVDF membranes (MP-PVDF). We also discovered that a high water contact angle
74 ($> 150^\circ$) alone did not entail resistance to scaling [27, 28], but slippage at the interface is more
75 critical in enhancing the anti-scaling performance. The slippage at the interface is essentially a
76 disruption to the static water layer in the laminar flow scenario [29, 30]. The disruption of the static
77 layer can be achieved by the change of hydrodynamics conditions, which may be achieved in this
78 context by the combination of a slippery membrane and a controlled pulse flow.

79 This work exploits the effects of pulse flow in maintaining the direct contact membrane
80 distillation performance subject to gypsum scaling. Tailored made micro-pillared PVDF

81 membranes with and without CF_4 surface modification were compared in the DCMD
82 concentrating process. Membrane surface slip characters, fouling, and flux patterns were examined
83 in order to elucidate the key factors in determining membrane fouling resistance, and thereby to
84 provide some guidance on both membrane and process design.

85

86 **2. Materials and methods**

87 **2.1 Materials and chemicals**

88 Polyvinylidene fluoride (PVDF, Solvay, Solef 1015) was used for preparing MP-PVDF. The
89 silicon wafer mold with a pillar array was kindly provided by Suzhou Crystal Silicon Electronic
90 and Technology. The pillars show dimensions of 5 μm in diameter (D), 10 μm in height (H) and
91 10 μm in period (P) [27, 28]. Polydimethylsiloxane (PDMS) and the curing agent (SYLGARD
92 184) were purchased from Dow Corning. Diethylene glycol (DEG, AR) and N,
93 N-Dimethylacetamide (DMAc, AR) were supplied by Sinopharm. Calcium chloride anhydrous
94 (CaCl_2 , AR) and sodium sulfate (Na_2SO_4 , AR) were supplied by Sigma-Aldrich. Procion Blue H-
95 5R was purchased from Alfa Aesar. All chemicals were used without further purification.

96 **2.2 Membrane preparation**

97 A tailored-made PDMS mold was replicated with complementary structure from a silicon
98 wafer with a micro-pillar structure following published procedures. It was then used for the
99 preparation of micro-pillared PVDF membrane (MP-PVDF) via a non-solvent induced phase
100 separation (NIPS) method [28].

101 CF₄ plasma treatment was employed to enhance the hydrophobicity of the MP-PVDF using
102 the plasma treatment system(IoN40, PVA Tepla Co. Ltd) based on our previous methods [31-33].
103 Briefly, the membrane subjected to a pretreatment under argon plasma at 45W/15 s and a CF₄
104 plasma at a glow discharge of 200W/15 min. The final membrane was denoted as CF₄-MP-PVDF.

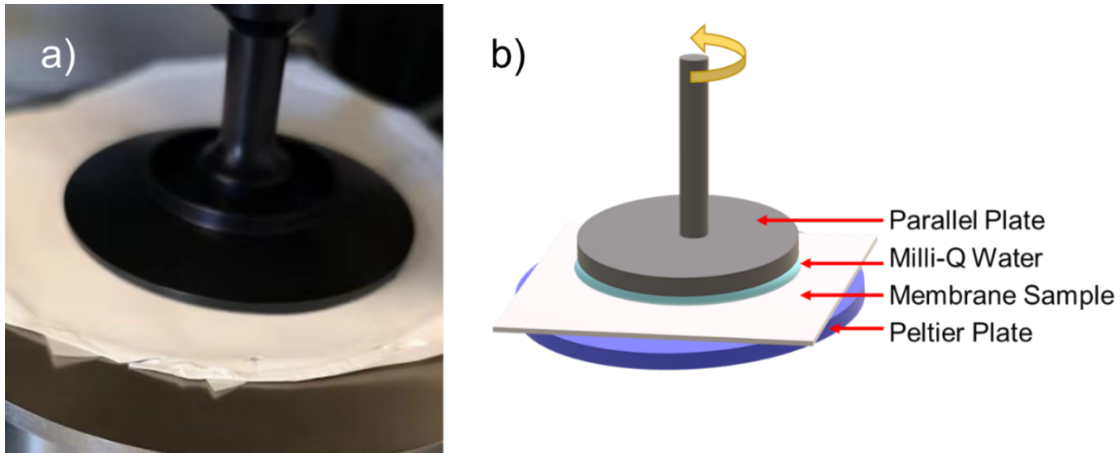
105 **2.3 Membrane characterization**

106 The surface wettability of the membranes was determined using a contact angle goniometer
107 (Maist Drop Meter A-100P). The membrane surface morphology was characterized via scanning
108 electron microscopy (SEM) (HITACH TM-1000). The pore size was measured using a capillary
109 flow porometry (Porolux 1000).

110 **2.3 Viscometry for wetting state**

111 The core of this experiment was to accurately measure the apparent viscosity of the water on
112 MP-PVDF and CF₄-MP-PVDF by a rheometer (AR-2000ex was shown in Supplementary
113 Information S2). As shown in Fig. 1, a membrane was carefully fixed to a Peltier Plate (a
114 semiconductor cooling sheet generally considered as a non-slip boundary) using double-sided tape.
115 1.7 mL Milli-Q water was dropped on the center of the sample. The gap between the stainless steel
116 parallel plate (diameter = 60 mm) and membrane surface was fixed at $h = 600 \mu\text{m}$ (auto set by
117 machine) [34]. The experiment was carried out at $23.0 \pm 0.1^\circ\text{C}$ and relative humidity of 64%.
118 Temperature and relative humidity are both very important for this measurement due to
119 temperature-sensitive viscosity and evaporation of water. At different shear rates, the torque
120 applied was tracked and the apparent viscosity of the liquid was then determined. The mean value

121 of four measurements was calculated as an average over the shear rate of 150 s^{-1} .



122
123 **Fig. 1.** (a) Photo of the test for apparent viscosity; The white was the membrane sample taped to
124 a stainless steel plate (thermostatically controlled); black plate above the membrane was the plate
125 connecting to the sensors; with shear rate in the range of 0 to 150 s^{-1} ; (b) Schematic of the
126 components for measurement. Milli-Q water was used as the probe liquid. The excess amount of
127 liquid was carefully removed using a tissue.

128

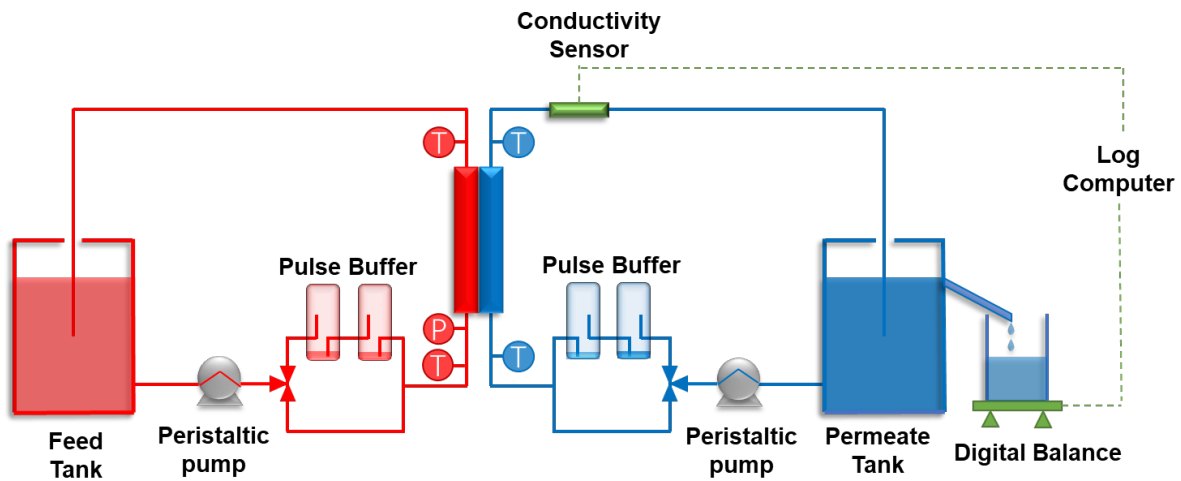
129 **2.4 Direct contact membrane distillation**

130 A bench-scale direct contact membrane distillation (DCMD) unit (Fig. 2) was used to evaluate
131 the scaling behavior with and without the pulse by peristaltic pumps and buffers. The peristaltic
132 pump rotates at 56 rpm in the feed side, which means the frequency is 2.8 Hz (56 r/min and three
133 pulses per rotation). By applying two buffers, the pulse from the peristaltic pumps was suppressed
134 (Fig. 2). The pulse buffer was an empty container of about 250 ml. After introducing liquid, the
135 buffer container was partly filled with liquid (liquid volume around 1/10 of the total). Due to the
136 large air volume, the pulse was suppressed and the flow after buffer became then steady. By trial-

137 and-error we figured out that two buffers were sufficient to create a rather steady flow. The feed
 138 was a calcium sulfate solution (2000 mg/L, prepared by mixing 14.7 mM CaCl₂ and 14.7 mM
 139 Na₂SO₄ solution). The original Saturation Index (SI) of the solution was 0.09. The SI was defined
 140 as the logarithm of the ratio of the Ion Activity Products (IAP) divided by the equilibrium constant
 141 (K_{sp}), respectively [35, 36]:

$$SI = \log \left(\frac{IAP}{K_{sp}} \right)$$

142
 143 The apparent SI with the different water recovery was shown in Figure 3 and calculated by using
 144 OLI Stream analyzer (OLI Systems, Inc., Morris Plans, NJ). The effective area of membranes for
 145 evaporation was 1000 mm² (50 mm in length, 20 mm in width and 3 mm in channel height). The
 146 same flow velocity of feed and permeate was maintained at 0.17 m/s. The resulting solution was
 147 supersaturated at 70 °C of 1.2 L. In this experiment, the surface with micro-pillars was in
 148 contact with the feed. The temperature of feed and permeate inlet solutions was maintained at 70
 149 ± 0.1°C and 20 ± 0.6°C, respectively. The water vapor flux (J , kg/m²·h) across the membrane was
 150 examined by measuring the permeate weight over time.



151

152 **Fig. 2.** Schematic diagram of the DCMD test unit. Membrane surface with pillars was facing the
153 feed solution. Both the feed and permeate flow rate was 600 mL/min. The rotating speeds of the
154 feed and permeate peristaltic pumps were measured to be 56 and 58 r/min, respectively.
155

156 **3. Results and discussion**

157 **3.1 Membrane characteristics**

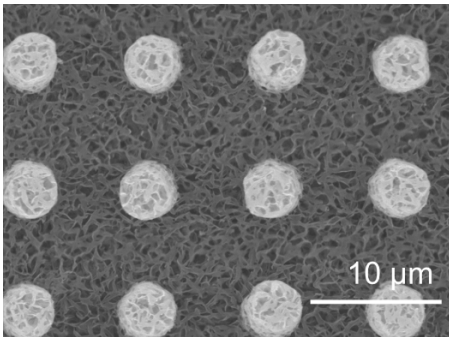
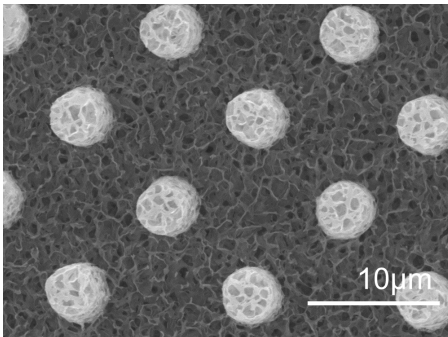
158 Table 1 lists the main surface properties of MP-PVDF and CF₄-MP-PVDF. CF₄-MP-PVDF
159 has a mean flow pore size of $0.201 \pm 0.013 \mu\text{m}$, higher than the pristine MP-PVDF (0.120 ± 0.005
160 μm), mainly caused by the plasma etching. Due to the hydrophobic nature of PVDF and the pillar
161 morphology, a very high static contact angle of $155.5 \pm 1.3^\circ$ was observed for the MP-PVDF.
162 Besides the CF₄-MP-PVDF showed an even higher static water contact angle of $165.5 \pm 1.7^\circ$,
163 which is ascribed to the CF₄ plasma treatment that has reduced the surface energy.

164 Table 1 shows that the sliding angle of MP-PVDF ($15 \pm 2.3^\circ$) is higher than that of CF₄-MP-
165 PVDF ($3.0 \pm 0.2^\circ$). Due to the etching effect and the deposition of the CF₄ plasma, the surface
166 energy of CF₄-MP-PVDF was lower than MP-PVDF [28, 31]. Moreover, lift-up effect reduces the
167 contact area between water and CF₄-MP-PVDF (or water-membrane-air three phase contact lines)
168 [32], thereby lowering the friction force and resulting in a low sliding angle. The low sliding angle
169 is an indication of low friction resistance to the rolling of water droplets. The static contact angle
170 may only reflect the balance of force in the gravity direction. Sliding measurement is very different
171 from the static contact angle in that it reflects the interaction between water molecules and

172 membrane surface in shear. The importance of the difference in the sliding angle may be correlated
 173 to the scaling behavior.

174

175 Table 1. The properties of MP-PVDF and CF₄-MP-PVDF surface

	MP-PVDF	CF ₄ -MP-PVDF
Contact angle/°	155.5 ± 1.3°	165.5 ± 1.7°
Sliding angle/°	15 ± 2.3°	3.0 ± 0.2°
Mean flow pore size/μm	0.120 ± 0.005	0.201 ± 0.013
Top view		

176

177 3.2 Membrane scaling and pulse flow

178 To evaluate the DCMD scaling performance of the two membranes, a supersaturated CaSO₄
 179 solution was used as the feed. For each membrane, steady flow and pulse flow were compared.

180 Fig. 3 shows the DCMD normalized water flux as a function of the water recovery ratio and the
 181 eventual membrane SEM images after DCMD experiments termination. As the water recovery
 182 increased, the feed solution was cumulatively concentrated followed by supersaturation. Under
 183 steady flow, both MP-PVDF and CF₄-MP-PVDF showed nearly the same induction time of about

184 13 h until a water recovery of 40%; after this point, MD flux quickly declined due to scaling.
185 Surface images confirmed that both membrane surfaces were covered by typical $\text{CaSO}_4 \cdot 2\text{H}_2\text{O}$
186 gypsum crystals (Fig. 3 a).

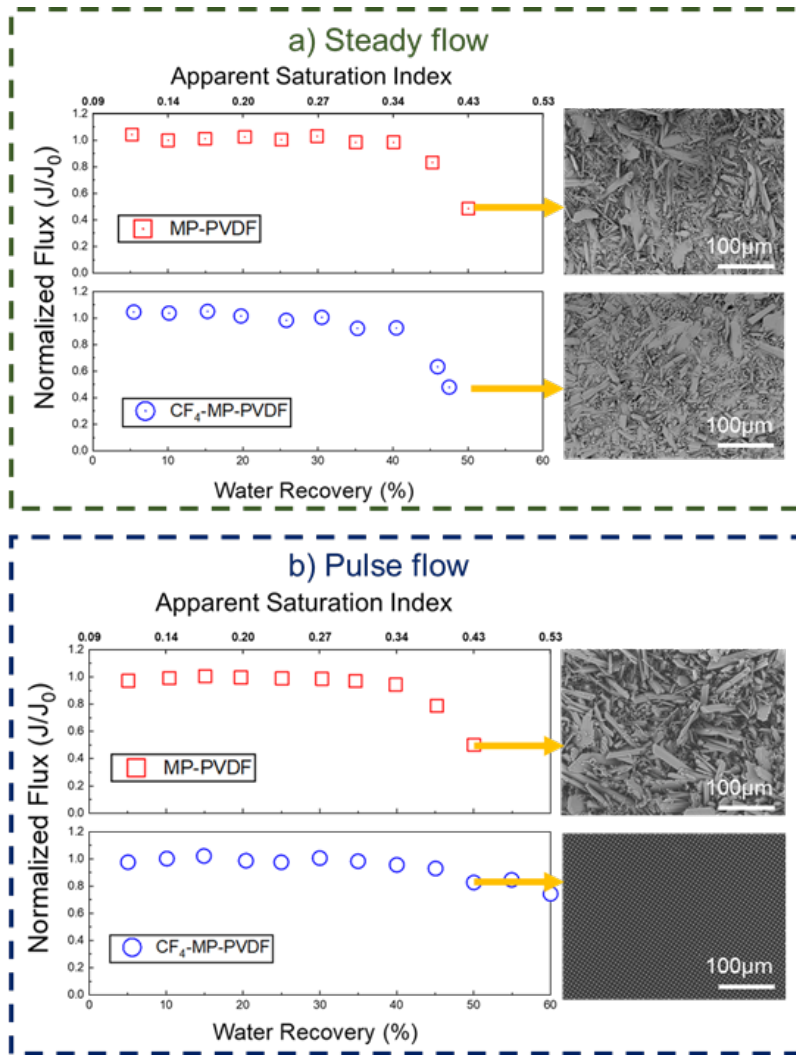
187 The intriguing result was significantly different MD performance of both membranes in case
188 of pulse flow from the peristaltic feed pump. MP-PVDF showed a very similar pattern in the flux
189 versus water recovery curve as that of the steady flow, but the CF_4 -MP-MVDF membrane
190 demonstrated an exceptionally stable MD flux till a water recovery of 60% at the end of the
191 experiment. It should be noted that the water recovery of 60% is the highest achievable result due
192 to limitation of the feed volume; above 60%, air would be pumped together with water to create
193 extra turbulence. At this recovery ratio, the feed salt concentration reached approximately 5000
194 mg/L ($2000/(1-60\%) = 5000 \text{ mg/L}$), far above the saturation point [37].

195 It is noteworthy that the flux declined gradually without a significant turning point in contrast
196 to those patterns of membranes that have crystals deposition when the water recovery reached 50%.
197 SEM imaging revealed a clean, nearly intact surface similar to the pristine one with no trace of
198 crystals (Fig. 3 b). We suspected that homogeneous nucleation or heterogeneous nucleation
199 occurred at around 40% water recovery by comparing the flux pattern turning points. For MP-
200 PVDF, under steady and pulse flow conditions, the crystals could precipitate or adhere to the
201 membrane surface, also for the CF_4 -MP-PVDF under steady flow. But at the pulse flow, for the
202 CF_4 -MP-PVDF, the crystals failed to adhere to the membrane surface though nucleation might
203 have occurred (i.e., the water recovery reached 50%), thus the membrane showed robust scaling

204 resistance under this circumstance. In addition, the permeate conductivity remained unchanged
205 indicating that no wetting occurred even though some of the membranes were scaled intensively.
206 At a water recovery rate of 60%, scaling was found for CF₄-MP-PVDF as shown in Supplementary
207 Information Fig. S4. Thus, the slight but gradual decline in MD flux was most probably a result of
208 partial scaling formation. This information was a further support for the scaling resistance of
209 slippery surface with pulse flow.

210 Based on both thermodynamic and hydrodynamic factors, one would expect that CF₄-MP-
211 PVDF had better scaling resistance than the MP-PVDF: (1) According to the conventional
212 thermodynamic model, very high contact angle and low surface energy corresponds to high scaling
213 resistance [13, 38]; (2) CF₄-MP-PVDF surface is slippery, thus less prone to scaling due to the
214 non-static liquid surface than MP-PVDF, a non-slippery membrane. However, Fig. 3 indicates that,
215 at a static non-pulse flow condition, slippery surface behaved similarly to the non-slippery surface
216 in scaling resistance. Furthermore, it seems that a combination of pulse flow and the slippery
217 surface is sufficient to resist scaling in DCMD. To unravel the above deductions, we need to first
218 quantify the interaction of the water and the membrane surfaces.

219



220

221 **Fig. 3.** Normalized water flux of the MP-PVDF (red squares) and CF_4 -MP-PVDF (blue circles)

222 membranes during MD operation at a) steady flow, b) pulse flow. The data for pulse flow was

223 adopted from reference [28]. SEM images of the membrane surfaces were taken when the water

224 recovery reached 50%. Arrows refer to the SEM image taken for the membrane at specific water

225 recovery. Permeate conductivity for all experiments remain constant, thus not shown here. The

226 initial flux J_0 of MP-PVDF and CF_4 -MP-PVDF were 32.0 and 31.1 $L\ m^{-2}\ h^{-1}$ in steady flow and

227 31.5 and 32.1 $L\ m^{-2}\ h^{-1}$ in pulse flow respectively.

228

229 **3.3 Wetting state**

230 Contact angle measurement gives only limited information as the water drops stay static on the
231 membrane surface. Any information on the wetting state at a dynamic condition would not be able
232 to be extracted directly from the results. The sliding angle using a water droplet reflects a
233 hydrodynamic interaction of water and membrane. It reflects the starting of the rolling off of a
234 water droplet; there is still a gap for the interaction of liquid and the membrane at a constant flow.
235 A rheology measurement called viscosimetry was utilized to quantify the hydrodynamic behavior
236 of water at the membrane surface. As shown in Fig. 4, here a simplified interfacial model is
237 introduced by assuming: (1) pillars are not wetted by water; thus, we do neglect the wetting state
238 of the pillars; (2) instead of a water-membrane interface, we identify a water-gas-membrane
239 (polymeric solid area) tri-phase interface (Fig. 4). In rheology measurement, a close-to-reality
240 simulation of the water-gas-membrane tri-phase interface would be constructed using a continuous
241 fluidic media. We expect to extract information close to the interface at DCMD.

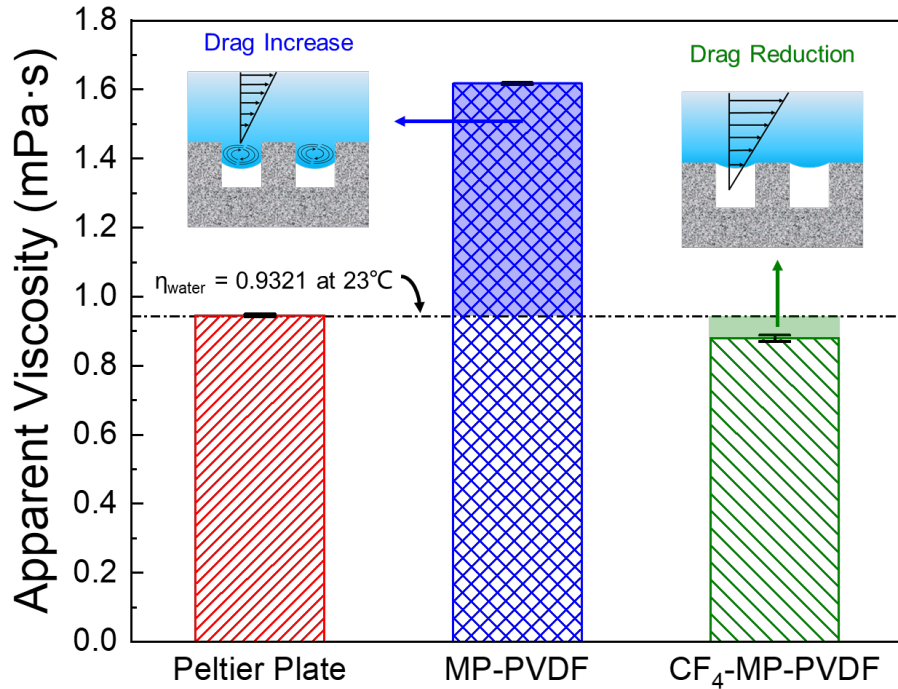
242 In Fig. 4, the apparent water viscosity measured at three different surfaces were compared:
243 Peltier Plate, MP-PVDF and CF₄-MP-PVDF. By definition, the water viscosity is measured on a
244 stainless steel Peltier Plate surface, which is presumably hydrophilic with a static water layer at
245 the water-plate interface during measurement. The measured viscosity of water was $\eta = 0.946 \pm$
246 0.004 mPa·s, within the experimental error for the literature reported value $\eta_{\text{water}} = 0.9321$ mPa·s
247 [39] (the red column in Fig. 4).

248 The relative deviation of the viscosity ($|\eta_{water}-\eta|/\eta_{water}$) in our work was 1.4%. Choi et al. [40]
249 claimed that the instrumental uncertainty in this measurement was within 0.5%, which required
250 precise control of liquid temperature, the setting resolution of torque and gap size. All these setting
251 controls were very difficult to be realized as we experienced in this work. The other work from
252 Bocquet et al. [41] benchmarked a standard deviation in torque using deionized water of 1.4% at
253 the shear rate of 150 s^{-1} . We took this as a more realistic validation of our results.

254 The second validation is that the experimental deviation of measurement is far below the
255 difference in the viscosity of Peltier Plate, MP-PVDF and CF_4 -MP-PVDF. For the surface, an
256 averaged apparent viscosity of MP-PVDF ($\eta = 1.617 \pm 0.003\text{ mPa}\cdot\text{s}$) corresponds to a 71%
257 increase (the light blue area in Fig. 4) to the value measured on the Peltier Plate. Since water is a
258 Newtonian fluid, such a drastic increase in the viscosity means an increase in drag for water by the
259 membrane surface [42]. However, for the CF_4 -MP-PVDF, an averaged apparent viscosity (η
260 $=0.879 \pm 0.009\text{ mPa}\cdot\text{s}$) (the light green area in Fig. 4) is 7% below the value measured on the
261 Peltier Plate. Conversely, this means that the CF_4 -MP-PVDF shows an obvious reduction in the
262 drag for water.

263

264



265

266 **Fig. 4.** Apparent viscosities of Milli-Q water measured for a gap of $h=600 \mu\text{m}$ on (i) Peltier Plate

267 surface; (ii) MP-PVDF surface; (iii) CF₄-MP-PVDF surface. The light blue area meant that water

268 reserved more drag due to the sagging water-gas interface which induced the vortex between the

269 pillars; The light green area meant that water flowed easily on the membrane due to the pinned

270 water-gas interface.

271

272 CF₄ plasma treatment to the MP-PVDF surface decreases the surface energy due to the

273 fluoropolymer deposition effect [33, 43]. Thus, it is logic that the CF₄ treated membrane showed

274 reduced drag to water in shear. By translating this hydrodynamic factor into a MD operation, the

275 water-gas interface is situated at a suspended state, as shown in Fig. 4. This lift-up state leads to

276 slippage. For MP-PVDF, although the morphology is nearly the same as the CF₄-MP-PVDF, a

277 significant increase in the drag in shear represents a severely sagging water-gas interface into the
278 pillars as shown in Fig. 4. Our observation was also confirmed by the literature reported results
279 [34]. Much higher drag of the MP-PVDF than that of the Peltier Plate is caused by the hydraulic
280 vortex flow in liquid below the pillars [44], resulting in significantly high apparent viscosity.

281 Apparently, this hydrodynamic measure under shear is very similar to the results found in the
282 sliding angle. Table 1 shows that the sliding angle of CF₄-MP-PVDF is about $3.0 \pm 0.2^\circ$, lower
283 than that of MP-PVDF ($15 \pm 2.3^\circ$). A simple geometry evaluation indicates that the sliding of a
284 water droplet occurs as the friction of the surface to the water droplet is equal to the gravity
285 component parallel to the surface. Thus, we obtain a ratio of friction force of the MP-PVDF to
286 CF₄-MP-PVDF about 5 ($= \sin(15^\circ)/\sin(3^\circ) = 4.95$). Or, a water droplet would find it much easier
287 to roll on a CF₄-MP-PVDF surface than on a MP-PVDF surface. This phenomenon is strongly
288 related to the wetting state at the surface.

289 As a summary, the wetting state and the hydrodynamic behavior of the water-gas interface
290 are clearly identified in a hydrodynamic condition. MP-PVDF is obviously in a pinned-wetting
291 state. The fluid at the pillar top area remains static, similar to a hydrophilic membrane. CF₄-MP-
292 PVDF, on the other hand, maintain a suspended wetting state. The water-gas interface remains
293 “floating” on the pillar top, thus contributing to slippage.

294

295 **3.4 Scaling resistance by synergy of pulse and slippage**

296 The experimental evidence showed that the CF₄-MP-PVDF is only scale resistant under pulse

297 flow condition. This result is exceptional. It highlights that membrane surface design and process
298 design are all critical. Very recent research work from Horseman et al [24] showed that air
299 scrubbing would allow stable MD operation, which is in practice of a prevention strategy. The
300 occurrence of nucleation of crystals is not fully prohibited. In this section, we will systematically
301 analyze the scientific origin of scaling resistance from membrane surface design and
302 hydrodynamic control.

303 Fig. 3 shows that the MP-PVDF is prone to scale. Combining with the drag measurement, the
304 occurrence of scaling is logic in that pinned wetting corresponds to a non-slip condition, or a static
305 layer at the membrane surface (here means the pillar top). Heterogeneous nucleation would occur
306 as CaSO_4 reaches saturation after a certain induction period of time. However, the CF_4 -MP-PVDF
307 showed nearly the same scaling behavior to the MP-PVDF, although the surface showed reduced
308 drag to water due to suspended wetting and slip (Fig. 4). This groundbreaking evidence means that
309 the slippery surface alone is not sufficient for scaling resistance.

310 The second result as shown in Fig. 3 is that pinned wetting state (MP-PVDF) plus pulse flow
311 is not scaling resistant either. But, a suspended wetting state with slippage (Fig. 4) appeared to be
312 scaling resistant. This difference might originate from the different gas-water interface.

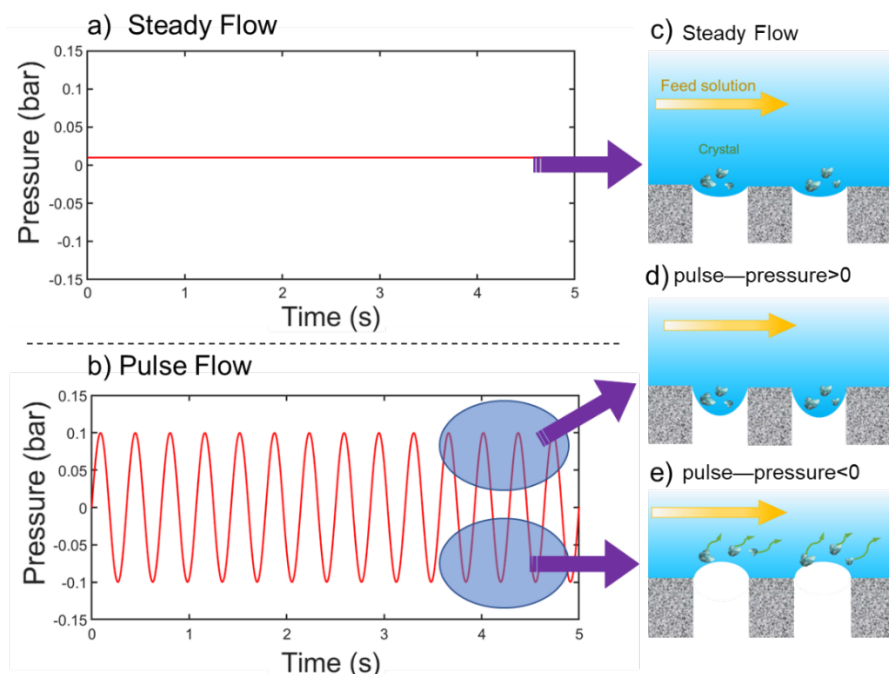
313 Fig. 5 outlines the pressure at the upstream of the feed test cell measured using an accurate
314 manometer (Fig. 2). When two pulse buffers were installed, very low positive constant pressure
315 about 0.01 bar was observed (Fig. 5 a); but without buffers, an oscillated pressure between
316 approximately 0.1(over-pressure) to -0.1 bar (under-pressure) was measured (Fig. 5 b). We noticed

317 that the over or under pressures when pulse flow was applied were nearly ten times as that at steady
318 flow. Pressure over ambient at the inlet of the test cell acts as a hydraulic pressure to drive water
319 into the small module inlet and maintain the velocity of the flow inside the small channel between
320 the membrane surface and the cell wall. Because water is an incompressible liquid, this pressure
321 is also applied to the fluid inside the test channel. At the module outlet, the pressure is close to the
322 atmosphere.

323 This means that the water-gas-membrane interface is not free of external force as always
324 assumed from a thermodynamic model, but rather under low over-pressure and forced to a lower
325 level as schematically depicted in Fig. 5 a. This sagging interface might reduce the slip effect of
326 the CF₄-MP-PVDF surface. Consequently, the interface becomes similar to that of a MP-PVDF.
327 As a result, the scaling resistance contributed by the suspended wetting and slip is diminished or
328 disappeared, as experimentally demonstrated in the same DCMD performance to the MP-PVDF
329 (Fig. 3).

330 Fig. 5 d,e schematically described the probable alteration of the water-gas interface in the gaps
331 of pillars in CF₄-MP-PVDF. Upon over-pressure, the interface sags down into the pillars; at under-
332 pressure, the interface lifts up in arching configuration (Fig. 5 e). The oscillation of the interface
333 follows the pulse of the peristaltic pump at a constant period of about 0.36 seconds ($= 60/(56*3)$
334 for 56 revolutions per minute produces and three pulses per revolution). This observation
335 corresponds well to previous findings from Duan et al. [45], where the configuration of the water-
336 gas interface alters under different pressure. The fluctuation of the water-gas interface on a slippery

337 membrane creates micro-scale hydrodynamic turbulence, which ultimately affects the aggregation
 338 of the scalants by homogeneous nucleation, and more importantly gives no residence time for the
 339 heterogeneous nucleation on the membrane surface. As a result, a robust sustainable scaling
 340 resistance is achieved.

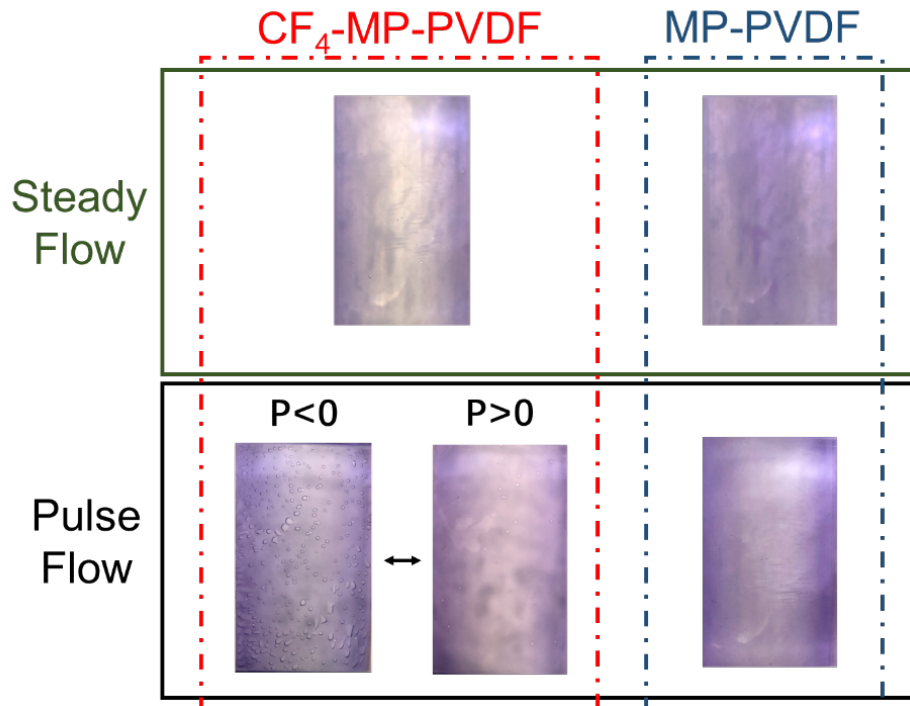


341
 342 **Fig. 5.** Schematic of scaling behavior for CF₄-MP-PVDF at steady and pulse flow. a) and b) Pressure
 343 versus time curve without and with pulse; the water-gas interface c) at steady flow; (d) with the pulse in
 344 positive pressure and (e) in negative pressure. The continuous line in (b) does not mean exact
 345 measurement but a linear regression of the pressure changes from negative to positive values.

346
 347 We attempted to visualize the interface fluctuation at over-pressure or under-pressure as shown
 348 in Fig. 5. It is unfortunate that we could not take sharp images at the interface yet. Thus, a
 349 macroscale image of the surface was taken to support above hypothesis. Fig. 6 shows the snapshots

350 of the membrane surfaces during MD operation. Obviously, at steady flow, a smooth, “static”
351 membrane surface was observed for both CF₄-MP-PVDF and MP-PVDF. But, at pulse flow,
352 unique surface bubbles were observed in the CF₄-MP-PVDF surface only at under-pressure, but
353 not at over pressure.

354 No visual difference could be identified for MP-PVDF at either under-pressure or over-
355 pressure (Fig. 6). The appearing of the bubbles in millimeter size at pulse flow is a result of
356 aggregation of many adjacent small bubbles (Fig. 5 e). After 2 h induction time, no bubbles were
357 seen, but CF₄-MP-PVDF maintained the scaling resistance for more than 20 h till a water recovery
358 of 50% (Fig. 3). This is an indirect, but sound proof of the “flip-flap” interface hypothesis as shown
359 in Fig. 5. We attempted to using light microscopy to obtain the images of this process. Due to the
360 instrument limit, modification of the experimental setup is under construction and our new results
361 would be reported in the near future.



362

363

364

365

366

367

368 4. Conclusions

369

370

371

372

373

Fig. 6. Observation of the MP-PVDF and CF₄-MP-PVDF surface with steady flow and pulse flow during MD. Procion Blue H-5R was added to feed at 100 mg/L. At steady flow, no bubbles were seen on either surfaces; At pulse flow, only CF₄-MP-PVDF surface showed bubbles at under pressure.

Synergy of feed flow patterns and wetting state related to slippery effect on the occurrence of scaling in DCMD was investigated based on micro-pillared PVDF membranes. MP-PVDF was found being prone to CaSO₄ scaling at both steady and pulse flows, but CF₄-MP-PVDF showed scaling at steady flow, but excellent scaling resistance at pulse flow by a clean surface and relatively stable MD flux at a supersaturation. Using rheological measurement, a significant

374 increase in the apparent viscosity of water for MP-PVDF corresponds to the pinned wetting with
375 a static water layer at the interface, but for CF₄-MP-PVDF, a slight decrease of apparent viscosity
376 indicates suspended wetting, thus surface slippage. At a steady flow, an over-pressure in feed
377 would forces the water-gas interface to sag into the pillars, thus creating a non-slip condition for
378 both MP-PVDF and CF₄-MP-PVDF, resulting in severe scaling. At a pulse flow, a pinned wetting
379 in MP-PVDF contributes to a static water-gas interface, but suspended wetting in CF₄-MP-PVDF
380 leads to a lift-up effect of the water-gas interface and avoids the scaling occurrence. Visualization
381 of the aggregated bubbles at the membrane surface at under-pressure in CF₄-MP-PVDF further
382 supports the above understanding. The results elaborate a scientific basis for the design of scaling
383 resistant membrane as a combination of superhydrophobic slippery surface plus a pulse flow. Our
384 findings provide a new strategy for the robust scaling MD process in the near future.

385 **Acknowledgements**

386 The research was partially supported by National Natural Science Foundation of China (No.
387 21978315, 21676290, 5191101572), and Newton Advanced Fellowship (Grant No. NA170113).
388 We also thank the frame work research consortium for partially financial support (RFBR No. 18-
389 58-80031, NSFC No. 51861145313, DST IPN/7864, NRT No.116020, CNPq/BRICS-STI-2-
390 442229/2017-8).

391 **Reference**

- 392 [1] A. Alkhudhiri, N. Darwish, N. Hilal, Membrane distillation: A comprehensive review, *Desalination*, 287 (2012)
393 2-18.
394 [2] K. Schneider, T.J. Vangassel, MEMBRANE DISTILLATION, *Chem. Ing. Tech.*, 56 (1984) 514-521.
395 [3] K.J. Lu, Z.L. Cheng, J. Chang, L. Luo, T.-S. Chung, Design of zero liquid discharge desalination (ZLDD) systems

396 consisting of freeze desalination, membrane distillation, and crystallization powered by green energies,
397 Desalination, 458 (2019) 66-75.

398 [4] T. Tong, M. Elimelech, The Global Rise of Zero Liquid Discharge for Wastewater Management: Drivers,
399 Technologies, and Future Directions, Environmental Science & Technology, 50 (2016) 6846-6855.

400 [5] A. Deshmukh, C. Boo, V. Karanikola, S. Lin, A.P. Straub, T. Tong, D.M. Warsinger, M. Elimelech, Membrane
401 distillation at the water-energy nexus: limits, opportunities, and challenges, Energy & Environmental Science,
402 11 (2018) 1177-1196.

403 [6] A.M. Alklaibi, N. Lior, Membrane-distillation desalination: status and potential, Desalination, 171 (2005) 111-
404 131.

405 [7] D.M. Warsinger, J. Swarninathan, E. Guillen-Burrieza, H.A. Arafat, J.H. Lienhard, Scaling and fouling in
406 membrane distillation for desalination applications: A review, Desalination, 356 (2015) 294-313.

407 [8] L.D. Tijing, Y.C. Woo, J.-S. Choi, S. Lee, S.-H. Kim, H.K. Shon, Fouling and its control in membrane
408 distillation—A review, Journal of Membrane Science, 475 (2015) 215-244.

409 [9] I.R. Salmon, P. Luis, Membrane crystallization via membrane distillation, Chemical Engineering and
410 Processing-Process Intensification, 123 (2018) 258-271.

411 [10] W.A. Johnson, R.F. Mehl, Reaction kinetics in processes of nucleation and growth, Transactions of the
412 American Institute of Mining and Metallurgical Engineers, 135 (1939) 416-442.

413 [11] A. Kullab, A. Martin, Membrane distillation and applications for water purification in thermal cogeneration
414 plants, Separation and Purification Technology, 76 (2011) 231-237.

415 [12] Z. Ma, Y. Hong, L. Ma, M. Su, Superhydrophobic Membranes with Ordered Arrays of Nanospiked
416 Microchannels for Water Desalination, Langmuir, 25 (2009) 5446-5450.

417 [13] V. Karanikola, C. Boo, J. Rolf, M. Elimelech, Engineered Slippery Surface to Mitigate Gypsum Scaling in
418 Membrane Distillation for Treatment of Hypersaline Industrial Wastewaters, Environmental Science &
419 Technology, 52 (2018) 14362-14370.

420 [14] E. Curcio, E. Fontananova, G. Di Profio, E. Drioli, Influence of the structural properties of poly(vinylidene
421 fluoride) membranes on the heterogeneous nucleation rate of protein crystals, Journal of Physical Chemistry
422 B, 110 (2006) 12438-12445.

423 [15] D. Erdemir, A.Y. Lee, A.S. Myerson, Nucleation of Crystals from Solution: Classical and Two-Step Models,
424 Accounts of Chemical Research, 42 (2009) 621-629.

425 [16] R. Zheng, Y. Chen, J. Wang, J. Song, X.-M. Li, T. He, Preparation of omniphobic PVDF membrane with
426 hierarchical structure for treating saline oily wastewater using direct contact membrane distillation, Journal of
427 Membrane Science, 555 (2018) 197-205.

428 [17] L.D. Tijing, Y.C. Woo, W.-G. Shim, T. He, J.-S. Choi, S.-H. Kim, H.K. Shon, Superhydrophobic nanofiber
429 membrane containing carbon nanotubes for high-performance direct contact membrane distillation, Journal
430 of Membrane Science, 502 (2016) 158-170.

431 [18] J. Lee, C. Boo, W.-H. Ryu, A.D. Taylor, M. Elimelech, Development of Omniphobic Desalination Membranes
432 Using a Charged Electrospun Nanofiber Scaffold, Acs Applied Materials & Interfaces, 8 (2016) 11154-11161.

433 [19] C. Boo, J. Lee, M. Elimelech, Omniphobic Polyvinylidene Fluoride (PVDF) Membrane for Desalination of
434 Shale Gas Produced Water by Membrane Distillation, Environmental Science & Technology, 50 (2016) 12275-
435 12282.

436 [20] Z. Wang, S. Lin, Membrane fouling and wetting in membrane distillation and their mitigation by novel

437 membranes with special wettability, *Water Research*, 112 (2017) 38-47.

438 [21] C. Zhu, G.L. Liu, C.S. Cheung, C.W. Leung, Z.C. Zhu, Ultrasonic stimulation on enhancement of air gap
439 membrane distillation, *Journal of Membrane Science*, 161 (1999) 85-93.

440 [22] G. Chen, X. Yang, R. Wang, A.G. Fane, Performance enhancement and scaling control with gas bubbling
441 in direct contact membrane distillation, *Desalination*, 308 (2013) 47-55.

442 [23] Y. Ye, S. Yu, L.a. Hou, B. Liu, Q. Xia, G. Liu, P. Li, Microbubble aeration enhances performance of vacuum
443 membrane distillation desalination by alleviating membrane scaling, *Water Research*, 149 (2019) 588-595.

444 [24] T. Horseman, C. Su, K.S.S. Christie, S. Lin, Highly Effective-Scaling Mitigation in Membrane Distillation Using
445 a Superhydrophobic Membrane with Gas Purging, *Environmental Science & Technology Letters*, 6 (2019) 423-
446 429.

447 [25] T. Zou, X. Dong, G. Kang, M. Zhou, M. Li, Y. Cao, Fouling behavior and scaling mitigation strategy of CaSO₄
448 in submerged vacuum membrane distillation, *Desalination*, 425 (2018) 86-93.

449 [26] H. Julian, Y. Ye, H. Li, V. Chen, Scaling mitigation in submerged vacuum membrane distillation and
450 crystallization (VMDC) with periodic air-backwash, *Journal of Membrane Science*, 547 (2018) 19-33.

451 [27] Z. Xiao, R. Zheng, Y. Liu, H. He, X. Yuan, Y. Ji, D. Li, H. Yin, Y. Zhang, X.-M. Li, T. He, Slippery for scaling
452 resistance in membrane distillation: A novel porous micropillared superhydrophobic surface, *Water Research*,
453 155 (2019) 152-161.

454 [28] Z. Xiao, Z. Li, H. Guo, Y. Liu, Y. Wang, H. Yin, X. Li, J. Song, L.D. Nghiem, T. He, Scaling mitigation in
455 membrane distillation: From superhydrophobic to slippery, *Desalination*, 466 (2019) 36-43.

456 [29] X.-M. Li, T. He, M. Crego-Calama, D.N. Reinhoudt, Conversion of a metastable superhydrophobic surface
457 to an ultraphobic surface, *Langmuir*, 24 (2008) 8008-8012.

458 [30] X.-M. Li, D. Reinhoudt, M. Crego-Calama, What do we need for a superhydrophobic surface? A review on
459 the recent progress in the preparation of superhydrophobic surfaces, *Chemical Society Reviews*, 36 (2007)
460 1350-1368.

461 [31] M. Tian, Y. Yin, C. Yang, B. Zhao, J. Song, J. Liu, X.-M. Li, T. He, CF₄ plasma modified highly interconnective
462 porous polysulfone membranes for direct contact membrane distillation (DCMD), *Desalination*, 369 (2015)
463 105-114.

464 [32] C. Yang, X.-M. Li, J. Gilron, D.-f. Kong, Y. Yin, Y. Oren, C. Linder, T. He, CF₄ plasma-modified
465 superhydrophobic PVDF membranes for direct contact membrane distillation, *Journal of Membrane Science*,
466 456 (2014) 155-161.

467 [33] X. Wei, B. Zhao, X.-M. Li, Z. Wang, B.-Q. He, T. He, B. Jiang, CF₄ plasma surface modification of asymmetric
468 hydrophilic polyethersulfone membranes for direct contact membrane distillation, *Journal of Membrane
469 Science*, 407 (2012) 164-175.

470 [34] S. Srinivasan, W. Choi, K.-C. Park, S.S. Chhatre, R.E. Cohen, G.H. McKinley, Drag reduction for viscous
471 laminar flow on spray-coated non-wetting surfaces, *Soft Matter*, 9 (2013) 5691-5702.

472 [35] R. Sheikholeslami, Assessment of the scaling potential for sparingly soluble salts in RO and NF units,
473 *Desalination*, 167 (2004) 247-256.

474 [36] K.S.S. Christie, Y.M. Yin, S.H. Lin, T.Z. Tong, Distinct Behaviors between Gypsum and Silica Scaling in
475 Membrane Distillation, *Environmental Science & Technology*, 54 (2020) 568-576.

476 [37] T.A. Hoang, H.M. Ang, A.L. Rohl, Effects of temperature on the scaling of calcium sulphate in pipes, *Powder
477 Technology*, 179 (2007) 31-37.

- 478 [38] E. Curcio, X. Ji, G. Di Profio, A.O. Sulaiman, E. Fontananova, E. Drioli, Membrane distillation operated at
479 high seawater concentration factors: Role of the membrane on CaCO₃ scaling in presence of humic acid,
480 Journal of Membrane Science, 346 (2010) 263-269.
- 481 [39] K.G. Nayar, M.H. Sharqawy, L.D. Banchik, J.H.V. Lienhard, Thermophysical properties of seawater: A review
482 and new correlations that include pressure dependence, Desalination, 390 (2016) 1-24.
- 483 [40] C. Chang-Hwan, C.J. Kim, Choi and Kim reply, Physical Review Letters, 97 (2006) 109602.
- 484 [41] L. Bocquet, P. Tabeling, S. Manneville, Comment on "Large slip of aqueous liquid flow over a
485 nanoengineered superhydrophobic surface", Physical Review Letters, 97 (2006) 109601.
- 486 [42] C. Navier, Mémoire sur les lois du mouvement des fluides, Mémoires de l' Académie Royale des Sciences
487 de l' Institut de France, 6 (1823) 389-440.
- 488 [43] G. Li, X. Wei, W. Wang, T. He, X. Li, Modification of unsaturated polyester resins (UP) and reinforced UP
489 resins via plasma treatment, Applied Surface Science, 257 (2010) 290-295.
- 490 [44] M.B. Martell, J.P. Rothstein, J.B. Perot, An analysis of superhydrophobic turbulent drag reduction
491 mechanisms using direct numerical simulation, Physics of Fluids, 22 (2010) 065102.
- 492 [45] S. Huang, P. Lv, H. Duan, Morphology evolution of liquid-gas interface on submerged solid structured
493 surfaces, Extreme Mechanics Letters, 27 (2019) 34-51.

494

Supplementary Information

Synergy of slippery surface and pulse flow: an anti-scaling solution for direct contact membrane distillation

Yongjie Liu ^{ab}, Zhansheng Li ^c, Zechun Xiao ^{bd}, Huabing Yin ^c, Xuemei Li ^b, Tao He^{*}

^aShanghai Advanced Research Institute, Chinese Academy of Sciences, Shanghai 201210, China

^bSchool of Physical Science and Technology, ShanghaiTech University, Shanghai 201210, China

^cUniversity of Chinese Academy of Sciences, Beijing 100049, China

^dNational Key Laboratory of Fine Chemical Engineering, Department of Polymer Materials, Dalian University of Technology, Dalian 116024, China

^eSchool of Engineering, University of Glasgow, Glasgow, G12 8LT, UK

*Corresponding authors: het@sari.ac.cn

S1 Wetting stability of pillared surface

We adopted the model from Xue's study [1] on the wetting stability of the submerged superhydrophobic. As shown in Fig. S1 a, we chose the classical Cassie-Baxter (CB) state as a reference, where a liquid-air interface is planar and the air trapped in a pore is at atmospheric pressure p_0 with a volume of $V_0 (= \pi R^2 H)$. The pore wall is assumed to be solid, not porous as in our case of membrane. At an external pressure of p_l , the air-liquid interface protrudes towards the pore and air is pressurizes inside (Fig. S1 b). When the sagging angle θ is equal to the advancing angle of the intrinsic material θ^* , a critical pressure p_l^c is obtained. If the pressure is above the critical pressure (p_l^c), the liquid-air interface is depinned and advances into the pores (Fig. S1 c).

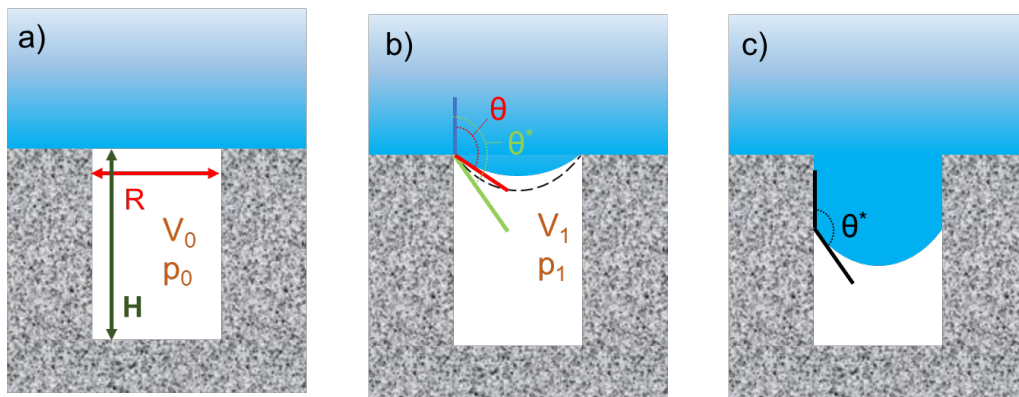


Fig. S1. Schematic illustration of the liquid–air interface in a hole at different state: (a) classical CB state; (b) at external over pressure, (c) after depinned and interface advances into the hole. The dashed line in (b) shows the critical positions of the advancing θ^* where the depinning occurs. R : pore radius; H : pore depth.

Based on the ideal gas law at a constant temperature, Eq. 1 and the Young-Laplace equation (Eq.

2) relates the meniscus curvature radius and the capillary pressure (the pressure difference across the water-air interface arising from the capillary forces) as

$$V_0 p_0 = V_1 p_1 \quad (1)$$

and

$$p_l = p_1 + \frac{2 \cos \theta}{R} \gamma \quad (2)$$

Where V and p represent the volume and pressure of air in the pore; the subscripts 0 and 1 denote the reference and final states of the air, respectively. γ is the surface tension of the liquid at the constant temperature. R is the radii of the hole. The volume of the liquid protruding into a pore is expressed as,

$$V_{in} = \frac{\pi R^3}{3 \sin^3 \theta} (2 - 3 \cos \theta + \cos^3 \theta) \quad (3)$$

The final volume of the air in the pore is

$$V_1 = V_0 - V_{in} = \pi R^2 H - \frac{\pi R^3}{3 \sin^3 \theta} (2 - 3 \cos \theta + \cos^3 \theta) \quad (4)$$

Combining Eq. 1-2 and Eq. 4 yields

$$p_l = p_0 / \left(1 - \frac{R}{3H \sin^3 \theta} (2 - 3 \sin \theta + \sin^3 \theta) \right) + \frac{2\gamma \cos \theta}{R} \quad (5)$$

Eq. 5 illustrates the equilibrium states as shown in Figure 1b with the three-phase contact line pinned at the top. When the liquid pressure is higher than the initial air pressure P_0 , the water-air interface will protrude downward into the pore. When the sagging angle reaches the advancing angle of the material, the pressure is named as the critical pressure. In other words, submitting θ^* for θ in Eq. 5, the critical pressure p_l^c is obtained.

For the pillared surface, corresponding effective geometric and capillary radius is approximate equivalent of the pore pattern surface. Based on Lobaton's work, the effective geometric radius refers to the volume of liquid protruding into each effective pore approximately equal to the volume of liquid

between four nearby pillars. For pillars on a square lattice (as shown in Fig. S2), the effective geometric radius is expressed as,

$$R_{eff}^g = \left(\sqrt{\frac{\pi}{2f}} - 1 \right) R_p \quad (6)$$

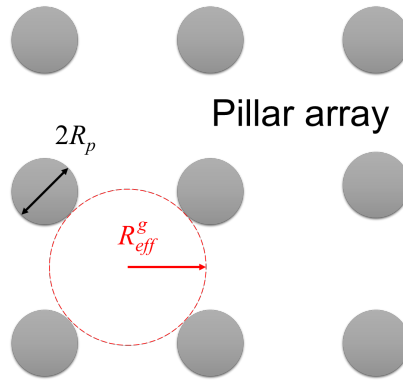


Fig.S2. Schematic illustrating the effective geometric radius R_{eff}^g for a structured surface with a pillar radius R_p (top view).

And the effective capillary radius for pillars on a square lattice [2]

$$R_{eff}^c = \frac{1-f}{f} R_p \quad (7)$$

Note that the values of R_{eff}^g and R_{eff}^c may differ greatly from each other, depending on the surface structure and solid fraction f .

R_{eff}^g and R_{eff}^c were substituted for R and the advancing angle θ^* is substituted for θ in Eq. 5. Then combined Eq. 5-7, Eq. 8 for the pillar substrates can be expressed as

$$p_i^c = p_0 / \left(1 + \frac{f}{(1-f)R_p^2 H} \frac{(R_{eff}^g)^3}{3 \cos^3 \theta^*} (2 - 3 \sin \theta^* + \sin^3 \theta^*) \right) - \frac{2\gamma \cos \theta^*}{R_{eff}^c} \quad (8)$$

Note that the height of those pillars is H. The parameters to calculate the critical pressures are shown in Table 1. The solid fraction f is equal to a pillar top surface area ratio to a period pattern area. The advancing angle of MP-PVDF and CF₄-MP-PVDF membranes were taken from the PVDF flat membrane and the CF₄ plasma treated PVDF flat membrane. This approximation is taken because of similar surface porous morphology of our tailor-made membrane to the commercial PVDF membrane. The surface tension of water is used.

Table S1. The parameters of MP-PVDF and CF₄-MP-PVDF to calculate the critical pressure

Membrane	$R_p / \mu\text{m}$	$H / \mu\text{m}$	f	$\theta^* / ^\circ$	p_0 / Pa	$\gamma / \text{mN}\cdot\text{m}$ (water at 70°C)
MP-PVDF	2.5	10	0.20	110	101325	64.4
CF ₄ -MP-PVDF	2.5	10	0.20	160	101325	64.4

The result of the critical pressure for MP-PVDF is 109.12 kPa and for CF₄-MP-PVDF is 131.33 kPa (both absolute pressures). This means that for MP-PVDF, water is depinned because the liquid pressure in membrane module is 0.1 bar (relative pressure) which is higher than the critical pressure; but for CF₄-MP-PVDF, water is still suspended because the liquid pressure is lower than the critical pressure.

S2 Photo of rheometer AR-2000ex

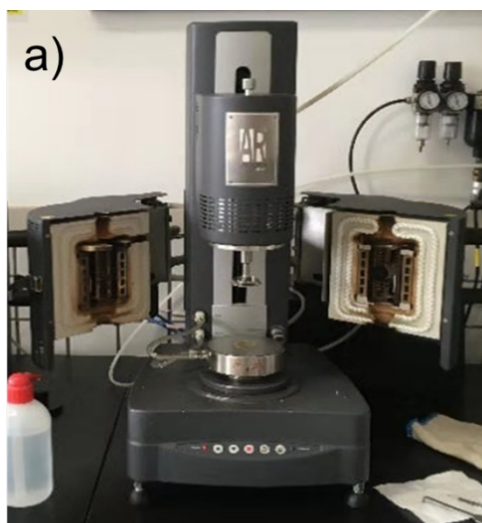


Fig. S3. Photo of the rheometer AR-2000ex used to confirm the wetting state of MP-PVDF and CF₄-MP-PVDF

S3 SEM image of fouled CF₄-MP-PVDF after MD under pulse flow.

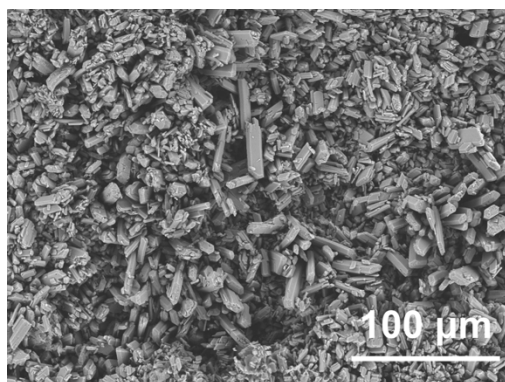


Fig. S4. SEM image of CF₄-MP-PVDF when the water recovery reached 60% under pulse flow.

Reference

- [1] Y. Xue, S. Chu, P. Lv, H. Duan, Importance of hierarchical structures in wetting stability on submerged superhydrophobic surfaces, *Langmuir*, 28 (2012) 9440-9450.
- [2] E. Lobaton, T. Salamon, Computation of constant mean curvature surfaces: Application to the gas-liquid interface of a pressurized fluid on a superhydrophobic surface, *Journal of colloid and interface science*, 314 (2007) 184-198.